

First-principles study of lattice instabilities in $\text{Ba}_x\text{Sr}_{1-x}\text{TiO}_3$

Ph. Ghosez*, D. Desquesnes[†], X. Gonze[†] and K. M. Rabe[‡]

**Institut de Physique, Université de Liège, Bât. B5, B-4000 Liège, Belgium*

†Laboratoire de Physico-Chimie et de Physique des Matériaux,

Université Catholique de Louvain, B-1348 Louvain-la-neuve, Belgium

‡Department of Physics and Astronomy, Rutgers University, Piscataway, NJ, USA

Abstract. Using first-principles calculations based on a variational density functional perturbation theory, we investigate the lattice dynamics of solid solutions of barium and strontium titanates. Averaging the information available for the related pure compounds yields results equivalent to those obtained within the virtual crystal approximation, providing frequencies which are a good approximation to those computed for a (111) ordered supercell. Using the same averaging technique we report the evolution of the ferroelectric and antiferrodistortive instabilities with composition.

INTRODUCTION

Ferroelectric solid solutions with perovskite structure can exhibit properties which are much more interesting for technological applications than those of the related pure compounds. This is the case for the new class of single crystal relaxor ferroelectrics, exhibiting exceptionally high piezoelectric constants [1]. It is also true for $\text{Ba}_x\text{Sr}_{1-x}\text{TiO}_3$ (BST), which combines a high dielectric constant with other properties making it a good candidate for the construction of dynamic random access memories (DRAM) [2].

In contrast to barium titanate (BaTiO_3) which is a prototype ferroelectric (FE), strontium titanate (SrTiO_3) is an incipient ferroelectric which undergoes an antiferrodistortive (AFD) phase transition at 105K [3]. Due to the different behavior of the related pure compounds, the structural properties of BST evolve with composition [4]. It exhibits a sequence of ferroelectric transitions similar to that of BaTiO_3 for Ba concentrations ranging from 20 to 100%. Close to pure SrTiO_3 the behavior is complicated by the competition between FE and AFD instabilities yielding the phase diagram reported in Ref. [4].

In the past few years, first-principles effective Hamiltonians successfully described the temperature-dependent behavior of various pure perovskite oxides [5]. The generalization of this theoretical approach to solid solutions is a new challenge

which includes some additional complications to treat the alloy disorder accurately.

A straightforward procedure is to try to extract the relevant information on the alloy from computation for various ordered supercells. This idea was applied to the study of $\text{Pb}_x\text{Ge}_{1-x}\text{Te}$ solid solutions [6] but has the inconvenience of being computationally intensive. An alternative and promising approach is based on the Virtual Crystal Approximation (VCA) which allows the retention of a crystal with the primitive periodicity but composed of virtual atomic potentials averaging those of the atoms in the parent compounds. A careful construction of the VCA for $\text{PbZr}_x\text{Ti}_{(1-x)}\text{O}_3$ yielded a stress induced phase transition [7] and a compositional phase boundary [8]. Going further, the construction of a model Hamiltonian based on VCA calculations for the same compound recently was used to describe most of its temperature-dependent properties [9]. In the latter case, the VCA calculation provided a reference structure to which corrections had to be added to treat the behavior of the real ions correctly.

If the purpose of the VCA is to define an average crystal from which the real solid solution can be described by including a restricted number of small corrections, one can ask if a similarly good estimate of the mixed compound could be obtained directly from the information available for the pure materials by averaging some *key* quantities. This idea is reinforced by the observation that the interatomic force constants seem very similar in the different ABO_3 compounds [10].

In what follows we define an Average Crystal Approximation (ACA) by averaging the lattice constant (a_{cell}), the Born effective charges (Z^*), the optical dielectric tensor (ϵ_∞), and the interatomic force constants in real space (IFC) of the pure compounds. We compare our results to those obtained (i) within the VCA and (ii) for a cubic ordered supercell with alternating planes of Ba and Sr along the (111) direction. We show that our ACA yields an excellent approximation to the dielectric and dynamical properties of the mixed compound. It allows the prediction of the lattice dynamics in the full range of composition without requiring any first-principles calculations other than those for the related pure compounds.

METHODOLOGY

General framework

Our calculations have been performed within the density functional theory [11] and the local density approximation, using the ABINIT package [12]. The ionic potentials screened by the core electrons have been replaced by highly transferable extended norm conserving pseudopotentials as proposed by M. Teter [13]. The Ba 5s, Ba 5p, Sr 4s, Sr 4p, Ti 3s, Ti 3p, Ti 3d, Ti 4s, O 2s and O 2p electrons have been treated as valence states. The wavefunction has been expanded in plane waves up to a kinetic energy cutoff of 45 Ha. The electronic exchange-correlation energy has been computed using a polynomial parametrization [14] of Ceperley Alder data [15]. Integrals over the simple cubic Brillouin zone have been replaced

by sums on a $6 \times 6 \times 6$ mesh of special k -points. A grid providing an equivalent sampling has been used for the supercell calculations.

The Born effective charges, the dielectric constants and the dynamical matrices have been computed within a variational formulation of the density functional perturbation theory [16]. The interatomic force constants in real space (IFC) and the phonon dispersion curves have been extracted following the scheme described in Ref. [17], which deals correctly with the long range character of the dipolar interaction. The IFC were obtained from the knowledge of the dynamical matrix on a $2 \times 2 \times 2$ BCC mesh of q -points.

Virtual atom pseudopotential

The virtual crystal approximation is based on the construction of a fictitious “virtual atom” potential by averaging the ionic potentials of the atoms alternating at the same site of the structure. As illustrated recently by Ramer and Rappe [7], there are different ways of combining non-local atomic pseudopotentials, each of them leading to different physical results. A careful choice seems necessary to predict accurately the alloy properties at the VCA level. However, this choice could be less stringent if we think about the virtual crystal as a reference structure from which the real crystal can be obtained by including a limited number of relevant corrections.

For BST, we choose therefore to stay with the most straightforward combination of the reference atomic pseudopotentials. The potential at the A-site can be formally defined for a concentration of $x\%$ of barium as:

$$V_{VCA}^{ps}[x] = xV_{Ba}^{ps} + (1 - x)V_{Sr}^{ps} \quad (1)$$

where V_{Ba}^{ps} and V_{Sr}^{ps} are the pseudopotentials of Ba and Sr atoms.

Non-local pseudopotentials, such as those we are using, can be expressed as a sum of a local contribution and short-range non-local corrections:

$$V^{ps}(r, r') = V^{loc}(r)\delta(r - r') + \sum_{l,m} \sum_q \frac{V_l^{ps} |\phi_{lm,q} \rangle \langle \phi_{lm,q} | V_l^{ps}}{\langle \phi_{lm,q} | V_l^{ps} | \phi_{lm,q} \rangle}. \quad (2)$$

Our virtual atom pseudopotential is then defined as follows [18]:

$$\begin{aligned} V_{VCA}^{ps}(r, r') &= [xV_{Ba}^{loc}(r) + (1 - x)V_{Sr}^{loc}(r)]\delta(r - r') \\ &+ \sum_{l,m} \sum_q \frac{xV_{Ba,l}^{ps} |\phi_{lm,q}^{Ba} \rangle \langle \phi_{lm,q}^{Ba} | xV_{Ba,l}^{ps}}{\langle \phi_{lm,q}^{Ba} | xV_{Ba,l}^{ps} | \phi_{lm,q}^{Ba} \rangle} \\ &+ \sum_{l,m} \sum_q \frac{(1 - x)V_{Sr,l}^{ps} |\phi_{lm,q}^{Sr} \rangle \langle \phi_{lm,q}^{Sr} | (1 - x)V_{Sr,l}^{ps}}{\langle \phi_{lm,q}^{Sr} | (1 - x)V_{Sr,l}^{ps} | \phi_{lm,q}^{Sr} \rangle} \end{aligned} \quad (3)$$

For x ranging from 0 to 1, our virtual atom evolves smoothly from Sr to Ba.

TABLE 1. Evolution of the LDA optimized lattice constant (bohr) with composition. Experimental values on the third line are interpolated from the data in the pure compounds using Vegard’s law.

	SrTiO ₃	x= 25%	x= 50%	x= 75%	BaTiO ₃
LDA/VCA	7.273	7.321	7.370	7.412	7.451
LDA/Supercell			7.366		
Experiment	7.38	7.43	7.47	7.52	7.56

GROUND-STATE PROPERTIES

First we focus on the lattice constant of the cubic perovskite structure and look at its evolution with composition. In Table 1, we report the LDA lattice constants for BaTiO₃ and SrTiO₃, for Ba_{1-x}Sr_xTiO₃ within the VCA (for x = 0.25, 0.50 and 0.75), and for the (111) ordered supercell. We compare the computed values with experimental results, which at intermediate compositions are accurately given by Vegard’s law [4]. While our results show the lattice constant underestimate typical of LDA, the Vegard’s law behavior is well reproduced.

We note that the theoretical LDA underestimate of the experimental lattice constant fortuitously corresponds to the effect of a similar external pressure of 8.7 GPa in both BaTiO₃ and SrTiO₃. In what follows, we will work at the experimental lattice constants which is therefore equivalent to imposing a fixed fictitious negative pressure of -8.7 GPa to the LDA results. For the mixed compounds we will work at the values obtained by Vegard’s law as reported on the third line of Table 1.

DIELECTRIC AND DYNAMICAL PROPERTIES

Born effective charges and dielectric tensor

In Table 2, we compare the Born effective charges and the macroscopic optical dielectric constants obtained in our various calculations. The values of O_{||} and O_⊥ refer respectively to the change of polarization for a displacement of the oxygen atom along the Ti–O direction and perpendicular to it.

We observe that the values of Z* and ϵ_∞ in the supercell are very similar to both those averaged from the pure compounds (ACA) and those obtained in the VCA. In particular, the ACA and the VCA similarly reproduce the large anomalous values of Z*_{Ti} and Z*_{O||} which play an important role in generating the FE instability. For Z*_A, both kinds of approximation yield the average of the values computed for Ba and Sr in the supercell. A similar observation was reported by Bellaiche *et al.* for PZT [9].

TABLE 2. Born effective charges and optical dielectric constant in the cubic perovskite structure. In the supercell, we can have either Ba or Sr at the A site: the first value refers to Ba, the second to Sr.

Atom	BaTiO ₃	SrTiO ₃	Average	VCA	Supercell
Z _A [*]	+2.74	+2.55	+2.64	+2.63	+2.71, +2.58
Z _B [*]	+7.32	+7.26	+7.29	+7.29	+7.29
Z _O [*]	-5.78	-5.74	-5.76	-5.75	-5.76
Z _{O_⊥} [*]	-2.14	-2.04	-2.09	-2.08	-2.09
ε _∞	6.75	6.33	6.54	6.51	6.54

Phonon frequencies and interatomic force constants

Finally we compare the phonon dispersion curves, yielding information at the harmonic level on the full lattice dynamics of the crystal. Phonon frequencies are obtained by diagonalizing the dynamical matrix. The latter is usually decomposed into a dipolar part computed from the values of Z^* and ϵ_∞ , and a short-range part computed using the IFC. Our ACA dynamical matrix is constructed by simply averaging all the previous quantities from their values in the pure compounds and using an average mass at the A-site, while the VCA requires a full set of additional first-principles calculations with the virtual atom potential.

In Fig. 1, we show the phonon dispersion curves of a mixed crystal of BST with $x=50\%$, obtained both within the ACA and the VCA. We compare the results to those obtained for the related pure compounds. The dispersion curves of BaTiO₃ were discussed in Ref. [20]. Those of SrTiO₃ have been recomputed and agree with the calculation reported previously by LaSota *et al.* [19]. Compared to BaTiO₃ which exhibits only a FE instability with a flat dispersion in the Γ -X-M plane, the FE instability in SrTiO₃ is more localized in q -space (around the Γ point) and coexists with an AFD instability extending along the Brillouin zone edges (R-M lines).

We observe that averaging the different quantities (Z^* , ϵ_∞ , IFC, atomic masses) does not yield an average of the phonon frequencies but rather is closer to the results for pure BaTiO₃. This is also what is found in the VCA, the two phonon dispersions being very similar. The major discrepancy appears for the low frequency Ti dominated branch along the Γ -M-X lines where the value of ω^2 , being near zero, is especially sensitive to small changes in the dynamical matrix.

In Table 3, we compare the ACA and VCA phonon frequencies at Γ and R in the reference perovskite structure to the related frequencies at the Γ point in the (111) ordered supercell. The different symmetry of the supercell does not allow a one to one correspondence but the comparison is made between phonons having the highest eigenvector overlap. We note that the supercell eigenmode associated with the R₁₅ modes of the perovskite structure, and involving displacement of the A atom, exhibits a small LO-TO splitting.

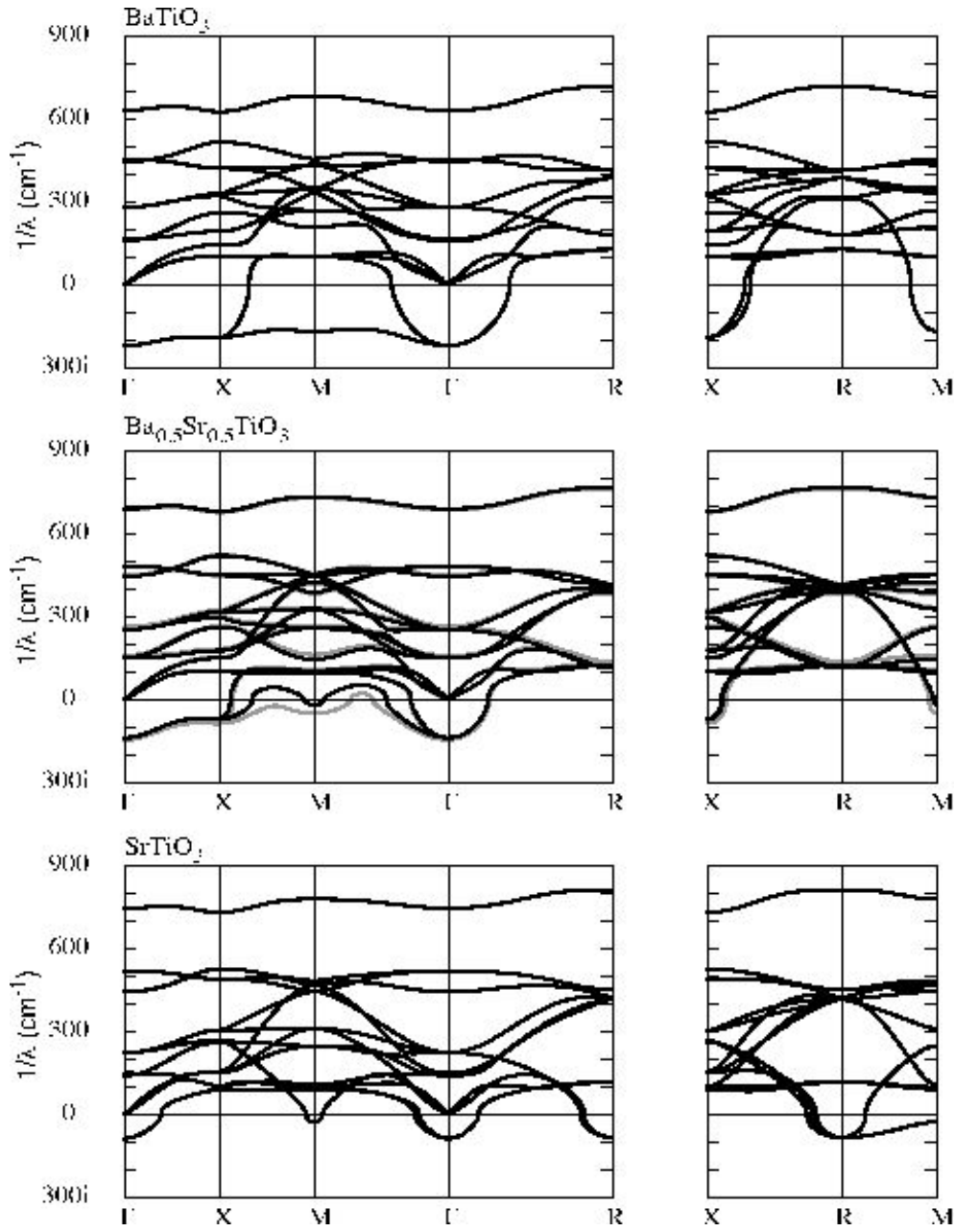


FIGURE 1. Phonon dispersion curves along high symmetry lines of the simple cubic Brillouin zone for BaTiO₃, Ba_{0.5}Sr_{0.5}TiO₃ and SrTiO₃. In the middle panel, the black lines correspond to the ACA, and the grey line to the VCA.

TABLE 3. Phonon frequencies (cm^{-1}) at the Γ and R points of the simple cubic Brillouin zone. Comparison of the ACA and VCA results with the supercell eigenmode at the Γ point which has the highest overlap with the corresponding ACA eigenvector.

Mode	BaTiO ₃	SrTiO ₃	Average	VCA	Supercell
$\Gamma_{15}(\text{TO})$	$219i$	$87i$	$138i$	$145i$	$151i$
$\Gamma_{15}(\text{A})$	0	0	0	0	0
$\Gamma_{15}(\text{LO})$	159	141	152	158	160
$\Gamma_{15}(\text{TO})$	166	149	152	159	161
Γ_{25}	281	223	253	263	272
$\Gamma_{15}(\text{LO})$	445	443	446	449	450
$\Gamma_{15}(\text{TO})$	453	519	482	481	480
$\Gamma_{15}(\text{LO})$	631	746	690	687	687
R_{25}	182	$84i$	135	114	86
R_{15}	128	118	131	125	110 – 111
$R_{12'}$	314	451	384	392	384
$R_{25'}$	386	418	405	406	404
R_{15}	414	423	419	415	412 – 418
$R_{2'}$	717	812	764	766	763

The overall agreement between ACA, VCA and supercell calculations is very good. This is particularly true for the Γ_{15} and $R_{25'}$ modes related to the FE instability. There is a larger discrepancy for the R_{25} AFD mode. We note however that projecting the supercell dynamical matrix within the subspace of the VCA eigenvector yields a value of 125 cm^{-1} (instead of 86 cm^{-1}) closer to VCA and ACA results. This shows that the discrepancy originates in a change of the eigenvector rather than in a modification of the interatomic force constants.

Evolution of the phonon instabilities with composition

As the ACA seems to give accurate results for the lattice dynamics of BST solid solutions, it offers an easy way to make a guess for the evolution of the FE and AFD instabilities with composition. We observe in Figure 2 that the square of the frequency of the R_{25} AFD mode evolves linearly with composition and becomes unstable for Ba concentrations smaller than 20 %. This corresponds precisely to the composition for which a change of behavior is observed experimentally in the phase diagram of BST [4]. In contrast, the FE instability exhibits a non-linear behavior and remains unstable for the full range of composition.

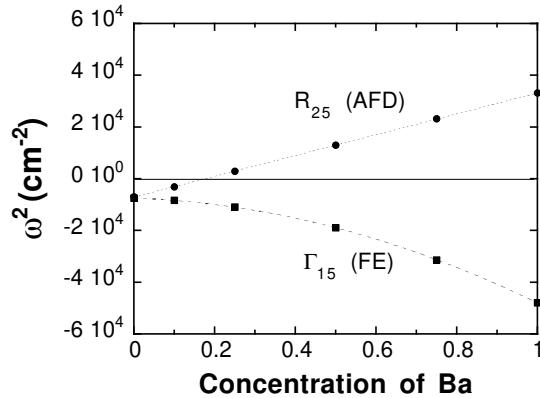


FIGURE 2. Evolution of the R_{25} and Γ_{15} unstable mode with composition, using the ACA.

CONCLUSIONS

In this paper, we have compared different approaches for the study of the lattice dynamics of BST solid solutions and have introduced a new Average Crystal Approximation. We have shown that the latter yields results equivalent to the VCA but with the advantage that it does not require any additional first-principles calculations if the information for the related pure compounds is available. Looking at the actual values of the IFC in the supercell could provide indications of the corrections to be included in the harmonic part of an effective Hamiltonian based on the ACA for the correct description of BST solid solutions.

ACKNOWLEDGMENTS

This work was supported by ONR grant No N00014-97-0047. Supercomputing support was provided by MHPCC. X.G. acknowledges financial support from the F.N.R.S. (Belgium), the F.R.F.C. (project 2.4556.99), the P.A.I. P4/10.

REFERENCES

1. Park S.-E., and Shrout T. R., *J. Appl. Phys.* **82**, 1804 (1997).
2. Bilodeau S. M., Carl, R., Van Buskirk P., and Ward J., *Solid State Tech.* **July 1997**, 235 (1997).
3. Lines M. E., and Glass A. M., *Principles and Applications of Ferroelectrics and Related Materials*, Oxford: Clarendon Press, 1977.
4. Lemanov V. V., Smirnova E. P., Syrnikov P. P., and Tarakanov E. A., *Phys. Rev. B* **54**, 3151 (1996).
5. Vanderbilt, D., *Curr. Opin. Solid State Mater. Sci.* **2**, 701 (1997).

6. Cockayne E., and Rabe K. M., in *First-principles calculations for ferroelectrics - Fifth Williamsburg Workshop*, ed. R. E. Cohen, Woodbury: AIP, Conference Proceedings **436**, 71 (1998).
7. Ramer N. J., and Rappe A. M., unpublished; *ibid.*, these proceedings.
8. Ramer N. J., and Rappe A. M., to appear in *Phys. Rev. B*.
9. Bellaiche L., and Vanderbilt D., to appear in *Phys. Rev. B* **61**, vol. 11 (2000); Bellaiche L., Garcia A., and Vanderbilt D., these proceedings.
10. Ghosez Ph., Cockayne E., Waghmare U. V., and Rabe K. M., *Phys. Rev. B* **60**, 836 (1999).
11. Jones R. O., and Gunnarsson O., *Rev. Mod. Phys.* **61**, 689 (1989).
12. ABINIT is a common project of the Université Catholique de Louvain, Corning Incorporated and other contributors, see the URL <http://www.mapr.ucl.ac.be/ABINIT> as well as Gonze X., Caracas R., Sonnet P., Detraux F., Ghosez Ph., Noiret I., Schamps J., these proceedings.
13. Teter, M. P., *Phys. Rev. B* **48**, 5031 (1993).
14. Goedecker S., Teter M., and Hutter J., *Phys. Rev. B* **54** 1703 (1996).
15. Ceperley D. M., and Alder B. J., *Phys. Rev. Lett.* **45**, 566 (1980).
16. Gonze X., Allan D. C., and Teter M. P., *Phys. Rev. Lett.* **68**, 3603 (1992); Gonze X., *Phys. Rev. B* **55**, 10337 (1997).
17. Gonze X., Charlier J.-C., Allan D. C., and Teter M. P., *Phys. Rev. B* **50**, 13035 (1994); Gonze X. and Lee C., *Phys. Rev. B* **55**, 10355 (1997).
18. Desquesnes, D., *Etude ab initio des solutions solides $Ba_xSr_{1-x}TiO_3$* , BSc thesis, Université Catholique de Louvain (1996).
19. LaSota C., Wang C.-Z., Yu R., and Krakauer H., *Ferroelectrics* **194**, 109 (1997).
20. Ghosez Ph., Gonze X., and Michenaud J.-P., *Ferroelectrics* **206**, 205 (1998)